frontiers in Physics

ORIGINAL RESEARCH
published: 12 April 2019
doi: 10.3389/fphy.2019.00052

Superconductivity and Its Enhancement in Polycyclic Aromatic Hydrocarbons

Guo-Hua Zhong[1,2], *Xiao-Jia Chen*[3*] *and Hai-Qing Lin*[2,4*]

[1] Shenzhen Institutes of Advanced Technology, Chinese Academy of Sciences, Shenzhen, China, [2] Beijing Computational Science Research Center, Beijing, China, [3] Center for High Pressure Science and Technology Advanced Research, Shanghai, China, [4] Department of Physics, Beijing Normal University, Beijing, China

The discovery of superconductivity above 30 K in aromatic hydrocarbons in the past years has been an exciting event in condensed matter physics, chemistry, and materials. Superconductivity was realized by simply introducing electrons in the network made by carbon and hydrogen—the two components for organic systems. However, the accurate amount of doped electrons and their positions have not been established experimentally. No agreement has been reached for the mechanism of their superconductivity. Here, the first-principles theory with the combination of electron correlations is used to address these problems. Our calculations show that both the single-ring compound (benzene) and the two benzene ring compound (naphthalene) are superconductors with transition temperatures (T_C's) of 6.2 K and 5.8 K, respectively, after administration of potassium. By examining the existing experimental data carefully, we find that there exists a unique superconducting phase with T_C in the range of 5 – 7 K for all aromatic hydrocarbons. The almost constant low density of states at Fermi level with about two-electron doping accounts for this unified phase. The high density of states at Fermi level upon three-electron doping seems responsible for the high-T_C phase in these hydrocarbons with long benzene rings. Meanwhile, the electronic correlations also increase with an increasing number of benzene rings. These findings offer clues to the understanding of the superconductivity as well as to the search of new superconductors in this family.

Keywords: aromatic hydrocarbons, benzene, naphthalene, superconductivity, electron-phonon coupling, electronic correlations, first principles

Edited by:
Shruba Gangopadhyay, University of Virginia, United States

Reviewed by:
Hamit Yurtseven, Middle East Technical University, Turkey
Rui-Qin Zhang, City University of Hong Kong, Hong Kong
Soham Ghosh, University of California, Davis, United States

***Correspondence:**
Xiao-Jia Chen
xjchen@hpstar.ac.cn
Hai-Qing Lin
haiqing0@csrc.ac.cn

Specialty section:
This article was submitted to Condensed Matter Physics, a section of the journal Frontiers in Physics

Received: *29 November 2018*
Accepted: *20 March 2019*
Published: *12 April 2019*

Citation:
Zhong G-H, Chen X-J and Lin H-Q (2019) Superconductivity and Its Enhancement in Polycyclic Aromatic Hydrocarbons. Front. Phys. 7:52. doi: 10.3389/fphy.2019.00052

1. INTRODUCTION

Organic materials with a crystal structure made primarily of a complex network based on carbon and/or hydrogen were postulated to superconduct with high transition temperature (T_c) and may even above room temperature [1]. Organic superconductors such as charge-transfer compounds are made up of electron donor molecules such as tetrathiafulvalene (TTF), bis-ethylenedithrio-TTF (BEDT-TTF, abbreviated as ET), and tetramethyltetraselenafulvalene (TMTSF) derivatives, as well as electron acceptor molecules such as tetracyanoquinodimethane (TCNQ) and fullerides [2–5], which were discovered many years ago and are being extensively studied. In 2010 and subsequent years, polycyclic aromatic hydrocarbons (PAHs) were found to exhibit superconductivity [6–9], and their discoveries have attracted great interest in these organic compounds. Experimental data showed that there usually exist multiple superconducting phases with different superconducting

transition temperature T_c, and the highest T_c seems to increase with the number of benzene rings within the unit cell [6–9]. These compounds all have a superconducting phase with $T_c \sim 5-7$ K. In addition, spin-liquid state has been also realized in an ionic PAH [10]. Recently, the crystal structures of potassium-intercalated PAHs have been experimentally determined [11]. This information is very useful in theoretical studies on the superconducting phase and for understanding the driving force for superconductivity. However, a systematic study on the superconductivity in PAH, e.g., the relation between T_c and the number of benzene rings, is lacking. The issue of what is the exact amount of the cation intercalation or doping into the PAHs to induce superconductivity remains unsettled. Benzene−, being the simplest aromatic hydrocarbon, has six carbons on a ring and six hydrogens attached, i.e., C_6H_6. Other PAHs are made of more benzene rings. Thus, being the basic unit of PAH, solid benzene stands out as an ideal system to start with and address relevant issues. A natural question is whether such a compound could superconduct when doped by alkali atoms. If it superconducts, will its properties mimic those of all aromatic hydrocarbons? What factor is important for higher T_c? Exploring structures of doped solid benzene and examining corresponding phase stability, followed by the study of superconductivity, are the tasks of this work.

Solid benzene, whose crystallization characteristics have been extensively investigated [12–14], has a rich phase diagram with evolution into several phases by changing temperature and pressure. Liquid benzene crystallizes at room temperature and about 0.07 GPa, in an orthorhombic phase with space group *Pbca* (phase I), containing four formula units (f.u.) per unit cell [12]. At 1.4 GPa, a transition occurs from phase I to phase II ($P4_32_12$), and then at 4 GPa, phase II transfers to phase III ($P2_1/c$), followed by phase IV (11 GPa) and phase V at higher pressures. Solid benzene has been found to be non-metallic and non-superconducting over a very broad pressure range. Upon heavy compression, solid benzene was predicted to undergo an insulator-to-metal transition in the pressure range of 180–200 GPa [15], suggesting that benzene is a possible superconductor under pressure. However, inherent to high-pressure techniques is the difficulty for experimental diagnosis and observation. Therefore, instead, we chose potassium (K) to dope solid benzene at ambient pressure and examine the possible realization of metallization and superconductivity. If doped solid benzene superconducts at ambient pressure, it would serve as an example to uncover the underlying origin of superconductivity in PAHs.

Although experimental studies on doping K into solid benzene have yet to be performed, the interaction between the benzene molecule and the K^+ ion has already been observed experimentally as well as studied theoretically by López et al. [16], a resource which implies the feasibility of doping potassium into solid benzene. Notably, doping potassium has been shown to be the most effective and common method to induce superconductivity in PAHs [6–9]. One reason is that K has a relatively low melting point as compared to other alkali elements, which makes the chemical reaction and crystallization from liquid states of K and benzene suitable.

2. MATERIALS AND METHODS

2.1. Structural Optimizations and Electronic Properties Calculation

All structural optimizations and electronic properties were calculated by using the Vienna *ab* initio simulation package (VASP) [17, 18]. In this work, the projector augmented wave (PAW) method [19] was adopted, and the exchange correlation energy was described by the Ceperley-Alder local density approximation (LDA) [20] as parameterized by Perdew and Zunger [21], which has been confirmed to be adequate by previous studies [22]. An energy cutoff of 500 eV was used for the plane wave basis sets. Thus, C-2*p*, H-1*s*, and K-3*p*4*s* were treated as valence states. The Brillouin zone (BZ) was sampled by $4 \times 4 \times 4$ Monkhorst-Pack *k*-point grids during the optimization, and double *k*-point in the electronic structural calculations. The convergence thresholds were set as 10^{-6} eV in energy and 0.005 eV/Å in force. A conjugate-gradient algorithm was used to relax the ions into their instantaneous ground state.

2.2. Electron-Phonon Interaction and Relevant Parameter Calculations

To calculate electron-phonon interaction and relevant parameters, we used the QUANTUM-ESPRESSO package (QE) [23] with a cutoff energy of 60 and 450 Ry for wave functions and charge densities, respectively. Forces and stresses for the converged structures were optimized and checked to within the error allowance of the VASP and QE codes. Troullier-Martins norm-conserving scheme [24] was used to generate the pseudopotentials for C, H, and K atoms. An $8 \times 8 \times 8$ Monkhorst-Pack *k*-point grid with Gaussian smearing of 0.03 Ry was used for the electron-phonon interaction matrix element calculations at $2 \times 2 \times 2$ *q*-point mesh.

3. RESULTS AND DISCUSSION

3.1. Prediction of Superconductivity in Benzene and Naphthalene

As a comparison and a check on accuracy, we start our investigation by looking at solid benzene. **Figure 1A** shows the optimized crystal structure of solid benzene from different orthographic directions, with crystal lattice constants $a = 7.041$ Å, $b = 8.903$ Å, and $c = 6.357$ Å at zero temperature and ambient pressure, which are 3–6% less than experimental values at 78 K [12]. If the effect of temperature is considered, the error between theoretical prediction and experimental measurement is acceptable. Solid benzene is a wide band gap insulator as shown in **Figure S1A**. Our calculated band gap of 4.1 eV is in good agreement with previous results [13]. From the reported data on PAHs, their superconductivity is highly sensitive to both the doping concentration and the cation positions in the unit cell. To examine both effects, we performed optimization studies on doped solid benzene, $K_xC_6H_6$, by varying potassium contents (x = 1, 2, 3) and the position of K atoms in the unit cell. The optimized crystal lattice constants and atomic coordinates are summarized in **Table S1**. The formation energy

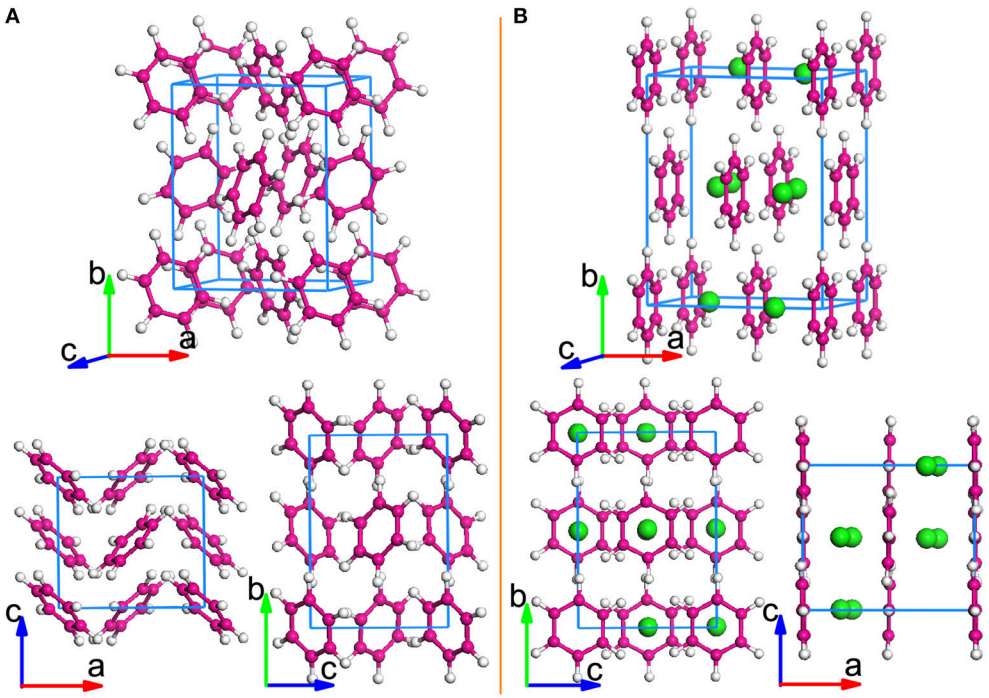

FIGURE 1 | Crystal structures of undoped and K-doped benzene. **(A)** Optimized crystal structures of solid benzene. **(B)** Crystal structure of K-doped solid benzene $K_2C_6H_6$. The structures are viewed from different axial directions. K-atoms are represented by Green spheres.

(E_f) is a good indication for examining the stability. We calculated the formation energy of the doped system using the following:

$$E_f = E_{K_xC_6H_6} - E_{C_6H_6} - x\mu_K(\text{bulk}) - x[\mu_K - \mu_K(\text{bulk})]$$

where $E_{K_xC_6H_6}$ and $E_{C_6H_6}$ is the total energy of the doped and host solid benzene, respectively. x is the number of doped K atoms. μ_K is the chemical potential of the K species. μ_K(bulk) can be obtained from the energy per K atom in the K metal with the *bcc* structure. When $\mu_K = \mu_K$(bulk), the doped element content is so rich that the related pure element phase can form. When $E_f < 0$, the doped compound can stably exist. The calculated result (see **Figure S2**) shows that $K_2C_6H_6$ has lower formation energy than $K_1C_6H_6$ and $K_3C_6H_6$ in a certain region of chemical potential, and its associated negative sign suggests easier synthesis.

Figure 1B shows the optimized $K_2C_6H_6$ crystal structure from different directions, with the following lattice constants: $a = 8.605$ Å, $b = 10.705$ Å, and $c = 6.415$ Å. When compared with the undoped case, we found that the lattice constants expand largely in the a and b directions. The insertion of eight K-atoms makes the volume expand by 26.9%. By K doping, a visible layered structure is formed, differing from that of the solid benzene. As shown in **Figure 1B**, all benzene rings are rotated and parallel to the *bc*-plane under the interaction of dopants, and K atoms are intercalated into two layers of benzene rings, occupying the Wyckoff 8*c* sites. The optimized structure of $K_2C_6H_6$ is found to tend toward the higher symmetry of *Fmmm* from the lower *Pbca* symmetry. Significantly, as shown in **Figure S3**, the layered structure of $K_2C_6H_6$ is similar to those of YbC_6 and CaC_6 [25]. This similarity indicates the possibility of superconductivity, because both YbC_6 and CaC_6 are known superconductors, with their T_c's reaching 6.5 K and 11.5 K, respectively [25, 26].

Once the crystal structure is determined, it is possible to obtain information about the electronic band structure. For $K_2C_6H_6$, eight conduction bands (called CB1, CB2, ... and CB8) along a high symmetry k-direction, $\Gamma - Z - T - Y - S - X - U - R$, of the Brillium zone are shown in **Figure 2A**. Specifically, under either *Pbca* or *Fmmm* symmetry, the lowest unoccupied molecular orbitals (LUMO) and LUMO+1 split into eight bands from Γ to Z, then they merge into four degenerate bands along the $Z - T - Y - S - X - U$ directions, and further into two highly degenerated bands along the $U - R$ direction. Electrons transferred from the K atoms to the C_6H_6 molecule occupy low energy orbitals and raise the Fermi level. Three bands—CB1, CB2, and CB3—are fully occupied by six of eight electrons, while the other three—CB4, CB5 and CB6—are partially filled by the remaining two electrons with Fermi level passing through. Both CB7 and CB8 are empty. Thus, $K_2C_6H_6$ is metallic but in the low-spin state. Compared with the solid benzene, we noticed that the intermolecular distance along benzene rings becomes smaller on the *bc*-plane of $K_2C_6H_6$. This effect enhances the intermolecular interaction and broadens the dispersion of energy bands. Analyzing the electronic characters near the Fermi level, as shown in **Figure 2B**, we found that the hole-like Fermi surfaces

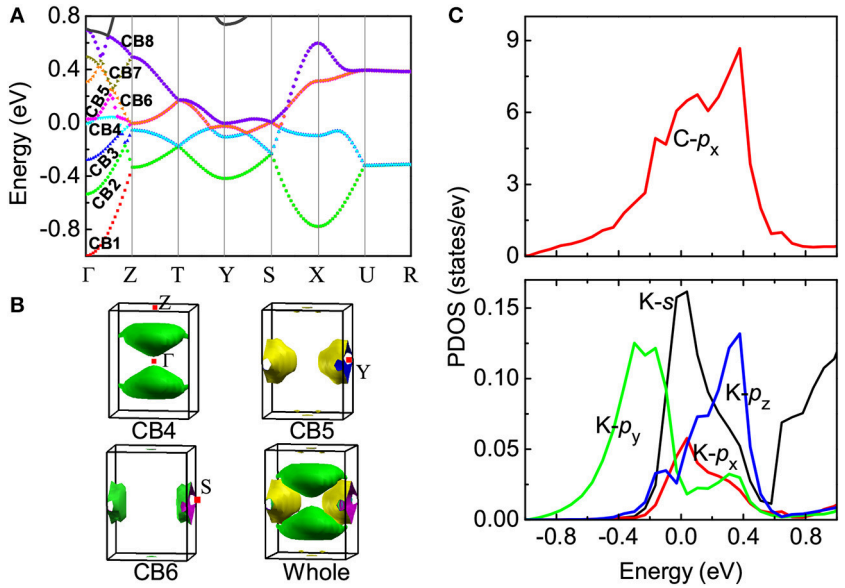

FIGURE 2 | Electronic band structure of $K_2C_6H_6$. **(A)** Energy band; **(B)** fermi surface; **(C)** projected density of states (PDOS), where zero energy denotes the Fermi level.

are formed by CB4 along the $\Gamma - Z$ k-direction, while both CB5 and CB6 contribute the electron-like Fermi surfaces around the Y k-point. Fermi surface nesting is quite clear. Calculation of the projected density of states (PDOS) shows that the C-p_y and C-p_z states are fully occupied and far below the Fermi level, while the C-p_x state has a large PDOS around the Fermi level, as shown in **Figure 2C**. Most PDOS of K-(s, p_x, p_y, p_z) states are above the Fermi level, indicating the electrons transfer from K to C-p_x orbital. The large ratio of C-p_x PDOS over K PDOS follows that C-p_x electronic states contribute more to the Fermi surfaces.

Next we examine whether this simplest aromatic hydrocarbon could exhibit superconductivity like other PAHs observed with superconductivity [6–9]. Assuming the pairing mechanism is still electron-phonon interaction mediated [22, 27], we evaluated the Eliashberg spectral function $\alpha^2F(\omega)$, the electron-phonon coupling integral $\lambda(\omega)$, and projected phonon density of states (PhDOS) of $K_2C_6H_6$ as a function of frequency. The results are shown in **Figure 3**. The vibration in the low frequency range of 0–250 cm^{-1} comes mainly from K, C, and H atom modes as shown in **Figure 3C**. The appearance of phonon modes of C and H atoms in the region of low frequency implies a weak intermolecular interaction. The modes with moderate frequencies of 300–1450 cm^{-1} are formed by C and H vibrations (**Figure 3C**), which results from the intramolecular interaction. The total λ is 0.67, which is comparable to that of $K_3C_{22}H_{14}$ [22] when assuming that the superconductivity in $K_3C_{22}H_{14}$ is mainly mediated by the electron-phonon interaction. As shown in **Figure 3B**, we also noted that vibrational modes from C and H atoms contribute 58% and 19% to the total λ value, respectively, while the remaining 23% is provided by the dopant phonon modes. Following the modified McMillan equation of Allen and Dynes [28], with the obtained values of $\lambda(\omega)$ and logarithmic average of phonon frequencies ω_{log}, and a typical value of 0.10 for the Coulomb pseudopotential $\mu^\star$, we obtained T_c = 6.2 K for $K_2C_6H_6$.

The dominant contribution to the total λ from the vibrational modes of the C atoms in $K_2C_6H_6$ shows some similarity with other C_6-based or low-carbon-bearing compounds. In reality, CaC_6 was discovered to exhibit superconductivity at 11.5 K [25]. Superconductivity has also been discovered in intercalation compounds of graphite with alkali metals AC_8 (A =K, Rb, or Cs) [29]. The predicted T_c of 6.2 K in $K_2C_6H_6$ is comparable to the temperature range of these low-carbon-based superconductors [25, 29].

Naphthalene ($C_{10}H_8$) is the second simple aromatic compound. Following the benzene crystal, a careful analysis on the 2-ring case also showed that K-doped naphthalene ($K_xC_{10}H_8$) possesses a superconducting phase with $T_c \sim$ 5.2 K comparable to the doped solid benzene. The crystal structures induced by doping are shown in **Figure S4** and the lattice parameters are listed in **Table S2**. $K_2C_{10}H_8$ was identified to be a more stable phase from the calculated formation energy result shown in **Figure S5**. As observed in solid benzene, the doping of two electrons per molecule is the most stable. Different from the metallicity in $K_2C_6H_6$, $K_2C_{10}H_8$ is a semiconductor with a band gap about 0.75 eV. Similar to charged chrysene ($C_{18}H_{12}$) [30] and picene ($C_{22}H_{14}$), however, naphthalene would become a metal if doped with two electrons with a small amount of charge fluctuations (see [24] and **Figures S6–S8**). For charged $K_2C_{10}H_8$, the Eliashberg spectral function $\alpha^2F(\omega)$ and the electron-phonon coupling integral $\lambda(\omega)$ as a function of frequency were also investigated (**Figure S9**). The values of λ = 0.64 and T_c = 5.8

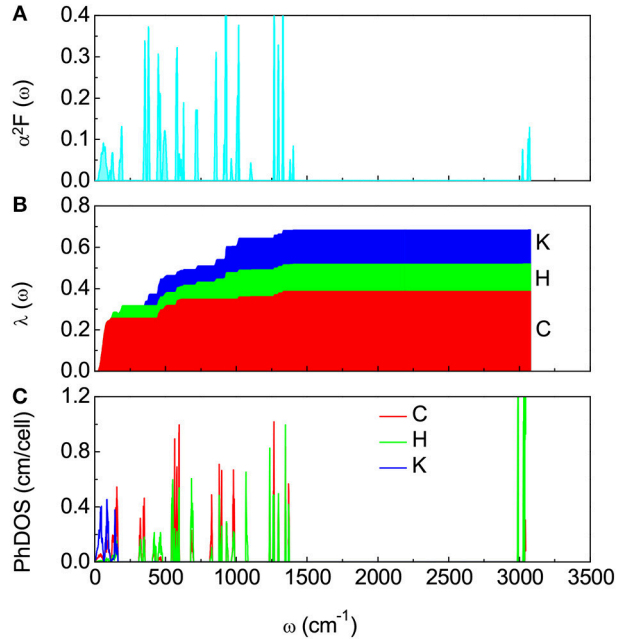

FIGURE 3 | Electron-phonon coupling and phonon density of states of $K_2C_6H_6$. **(A)** Electron-phonon coupling Eliashberg spectral function $\alpha^2F(\omega)$. **(B)** Electron-phonon coupling integral $\lambda(\omega)$ resolved by projections on C, H, and K phonons. **(C)** Phonon density of states (PhDOS) of $K_2C_6H_6$ projected on C, H, and K modes.

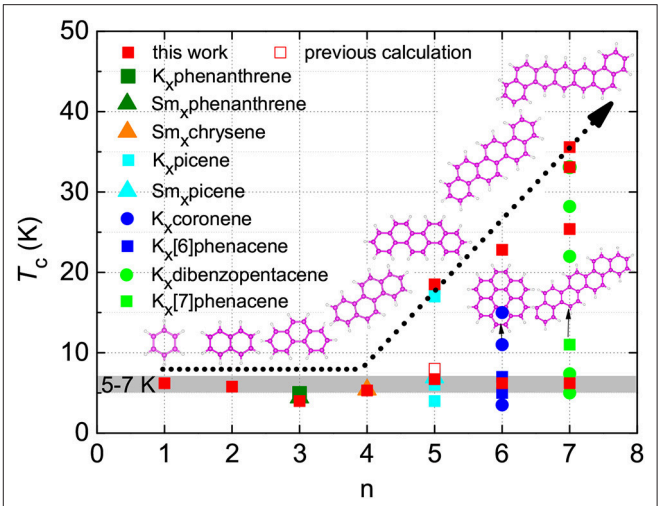

FIGURE 4 | Superconducting transition temperatures of aromatic hydrocarbons. Variation of superconducting transition temperature T_C with the number of benzene rings (n) for various aromatic hydrocarbons. The gray region is the guide for eyes. Solid red squares represent our predicted results, while the hollow red square implies the predicted result by Casula et al. [22] Other data are taken from experiments.

K ($\mu^\star = 0.1$) were obtained for the $K_2C_{10}H_8$ charged with the 0.1e per molecule. These calculated results on superconductivity of doped naphthalene have similarities with those of doped benzene.

3.2. Variation of Superconducting Transition Temperature Among Aromatic Hydrocarbons

By the same approach mentioned above, we have also investigated the superconductivity of K-doped phenanthrene ($K_xC_{14}H_{10}$). The theoretically predicted T_c for this material is marked out in **Figure 4**, which is in good agreement with the experimental value. The calculated superconducting parameters of $K_xC_{14}H_{10}$ are presented in **Figure S10C** and **Table S3**. A comparison of the predicted superconducting of benzene, naphthalene and phenanthrene with other PAHs reveals a common feature of aromatic hydrocarbons (**Figure 4**). Besides the reported high-T_c phases with $T_c = 18$ K for K-doped picene ($K_xC_{22}H_{14}$) [6], 15 K for K-doped coronene ($K_xC_{24}H_{12}$) [7], and 33 K for K-doped 1,2:8,9-dibenzpentacene ($K_xC_{30}H_{18}$) [9], multi-superconducting phases in long-benzene-ring hydrocarbons were generally observed. A low T_c phase with almost the same T_c range, $5-7$ K, exists in these hydrocarbon superconductors discovered so far [6–9]—5 K for $K_xC_{14}H_{10}$ [8], 7 K for $K_xC_{22}H_{14}$ [6, 7], and 7.4 K for $K_xC_{30}H_{18}$ [9]—though several other transitions with higher T_c's were also observed. T_c of $5-7$ K was also reported for $K_xC_{24}H_{12}$ [7] in addition to three other transitions. Moreover, both $Rb_3C_{22}H_{14}$ and $Ca_{1.5}C_{22}H_{14}$ show the superconducting transition at temperatures around 7 K [6]. In particular, Sm-doped phenanthrene, chrysene and picene show the superconductivity around $T_c \sim 5$ K [31]. It is important to note that the superconducting transitions were readily observed in the temperature range of $5-7$ K for all reported aromatic hydrocarbons with various numbers of benzene rings. These observations are in good agreement with our current prediction for benzene, naphthalene, and phenanthrene, the relatively simple compounds of this series. So a natural question is what accounts for this most common low-T_c phase and why the compounds with multiple benzene rings have high-T_c phases.

For the number of benzene rings from one to seven, we have compared the growth situations of all aromatic hydrocarbons based on the calculated formation energies shown in **Figures S11**, **S12**. For K-doped phenanthrene shown in **Figure S11C**, similar to benzene and naphthalene, $K_2C_{14}H_{10}$ is more stable in the chemical potential region satisfying $E_f < 0$. Hence, we suggest that the superconducting phase of $T_c \sim 5$ K observed by experiment [8] is $K_2C_{14}H_{10}$ instead of $K_3C_{14}H_{10}$. For K-doped chrysene ($K_xC_{18}H_{12}$), a four-benzene-ring system, our previous study [30] has indicated that $K_2C_{18}H_{12}$ is the most stable case in the chemical potential region satisfying $E_f < 0$ (Also see **Figure S11D**). As a result, when intercalating two K atoms, the doped system is the most stable for benzene, naphthalene, phenanthrene, and chrysene. Here, we call them short-benzene-ring systems. Differing from these short-benzene-ring systems, satisfying $E_f < 0$, as shown in **Figure S12A**, $K_2C_{22}H_{14}$ firstly obtains stable phase with the increase of K chemical potential, and then, under the K-rich limited condition, the high-concentration doping phase of $K_3C_{22}H_{14}$ can also be obtained. The same

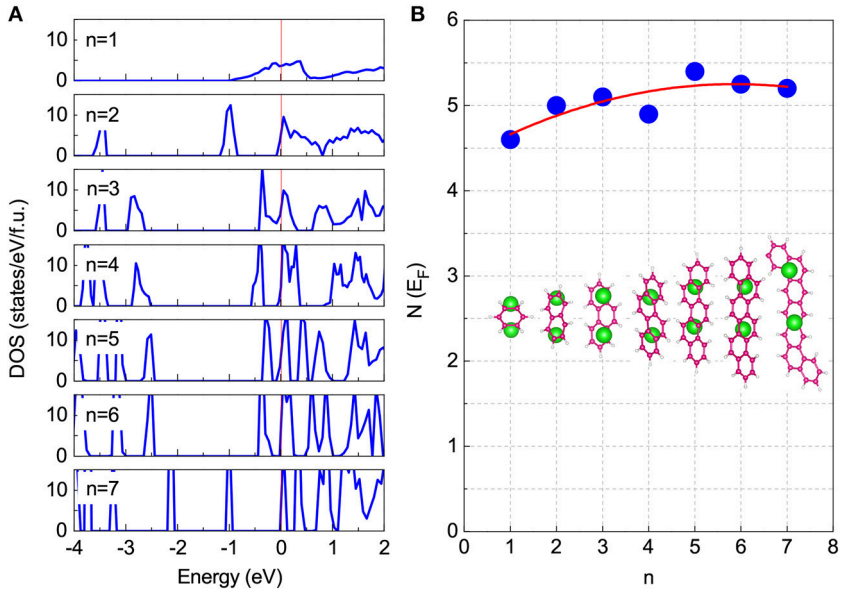

FIGURE 5 | Total density of states (DOS) for K_2-doped cases. *n* represents the number of benzene rings in system. These systems include $K_2C_6H_6$ (*n* = 1), charged $(K_2C_{10}H_8)^{+0.1e}$ (*n* = 2), $K_2C_{14}H_{10}$ (*n* = 3), charged $(K_2C_{18}H_{12})^{+0.1e}$ (*n* = 4), charged $(K_2C_{22}H_{14})^{+0.1e}$ (*n* = 5), charged $(K_2C_{26}H_{16})^{+0.1e}$ (*n* = 6), and charged $(K_2C_{30}H_{18})^{+0.1e}$ (*n* = 7), respectively. **(A)** The results of DOS for K_2-doped cases are presented. Zero energy denotes the Fermi level. **(B)** The DOS at Fermi level ($N(E_F)$) varies with *n*. The corresponding structures are also inserted.

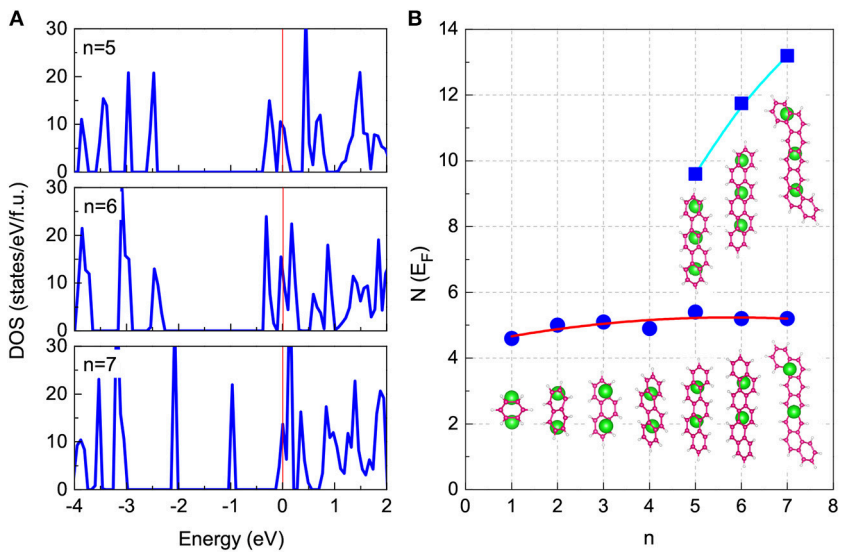

FIGURE 6 | Total DOS for K_3-doped cases with the long-benzene-ring chain. **(A)** The results of DOS for K_3-doped cases of $K_3C_{22}H_{14}$, $K_3C_{26}H_{16}$, and $K_3C_{30}H_{18}$ are presented. Zero energy denotes the Fermi level. **(B)** The $N(E_F)$ of K_3-doped cases is compared with that of K_2-doped cases. The corresponding structures are also inserted.

situations also occur in K-doped [6]phenacene ($K_xC_{26}H_{16}$) and $K_xC_{30}H_{18}$ (See **Figure S12**). Thus we put picene, [6]phenacene, and 1,2;8,9-dibenzopentacene in the same class as long-benzene-ring systems. From these calculated results, for short-benzene-ring systems, the doping of two electrons is the most stable, while for long-benzene-ring systems, both the dopings of two and three electrons are, respectively, the more stable phase in the different regions of K chemical potential. Thus, the doping phases with different K contents can be obtained in long-benzene-ring systems. However, in all aromatic hydrocarbons, stability with two-electron doping is a common feature. The unified phases with two-electron dopant for all the studied compounds in this series are consistent with recent experiments [11].

TABLE 1 | Based on the LDA, the calculated band gap (E_g) is smaller than the experimental one for each PAH. Reproducing the experimental band gap, the values of the μ and ν parameters are presented.

	3rings-A	4rings-A(B)	5rings-A	6rings-A	7rings-A	5rings-B	6rings-B	7rings-B
E_g (expt.)	3.16	3.3	3.3	3.15	3.2	3.3	3.2	3.2
E_g (LDA)	2.80	2.40	2.31	2.07	2.04	2.20	1.82	1.03
ν (HSE, $\mu = 0.1$)	0.05	0.18	0.21	0.25	0.26	0.27	0.36	0.62
ν (HSE, $\mu = 0.2$)	0.10	0.26	0.30	0.36	0.37	0.40	0.55	0.91

The experimental results of band gaps are taken from previous reports [7, 42–46].

With these analyses above, we are confident to conclude that the presence of the superconducting phase with T_c around $5-7$ K is a common feature of all aromatic hydrocarbons. In most cases, the low-T_c phase was easily fabricated and more stable than the higher T_c phase [6, 7, 9]. Considering the fact that the cation concentration has never been experimentally identified by using the reliable neutron scattering or single crystal X-ray diffraction techniques, all the reported doping levels are an ideal chemical estimation based on the synthesis procedure. Our phase stability examination for K-doped aromatic hydrocarbons pins down the doping concentration of the exact two electrons for the stable superconducting phase of these hydrocarbons with T_c of $5-7$ K. The superconducting phase with high-T_c is apparently the characteristic feature of long-benzene-ring systems, tending toward high-concentration doping such as three or more electrons.

In addition, we have investigated the density of states at Fermi level ($N(E_F)$) to analyze the origin of this unified superconducting phase, since the stable phase of low-concentration doping can be obtained in all aromatic hydrocarbons. As shown in **Figure 5**, the low-concentration K_2-doping results in small and comparable values on the $N(E_F)$ for all aromatic hydrocarbons. Moreover, the obtained ω_{log} values of 199.8 K for $K_2C_6H_6$, 210.4 K for charged $K_2C_{10}H_8$, and 193.7 K for $K_2C_{14}H_{10}$ are also comparable in quantity with 207 K of $K_3C_{22}H_{14}$ as shown in [19]. These results indicate that almost the same strength of electron-phonon coupling exists in all the K_2-doping cases. Based on the superconductivity mediated by the electron-phonon interaction, we suggest that the unified superconducting phase of $5-7$ K mainly comes from the low and the almost-same $N(E_F)$ value induced by two-electron doping. The electron-phonon interaction is enough to describe the superconductivity of this unified superconducting phase. With the help of the analysis of stability and DOS at the Fermi level above, we predict that the T_c of K-doped chrysene is in the range of $5-7$ K as shown in **Figure 4**. Although a complete understanding of the mechanism of superconductivity in aromatic hydrocarbons is yet to be achieved, the common feature of the $5-7$ K superconducting phase for all reported aromatic hydrocarbons provides important clues for understanding the superconductivity itself as well as for the search of new superconductors in this series.

For long-benzene-ring systems, multi-doping concentrations are feasible. At a high-concentration doping level, as shown in **Figure 6**, K_3-doping clearly leads to larger values of $N(E_F)$ compared with K_2-doping. Within the framework of the BCS theory, K_3-doping can drive a stronger electron-phonon interaction to exhibiting higher-T_c superconductivity. Hence, for each long-benzene-ring system, this high-T_c phase is related to the high $N(E_F)$ value induced by the three-electron doping. Regarding the enhancement of superconductivity among aromatic hydrocarbons, this is also related to the increase of the $N(E_F)$ with the number of benzene rings as shown in **Figure 6B**. Based on the discussion above combining the stability with the values of $N(E_F)$, we predicted that the T_c of K_2-doped PAHs is in the range of $5-7$ K, while the T_c of $K_3C_{22}H_{14}$, $K_3C_{26}H_{16}$, $K_3C_{30}H_{18}$, $K_{3.17}C_{30}H_{18}$, and $K_{3.45}C_{30}H_{18}$ is 18.5, 22.8, 25.4, 33.1, and 35.6 K, respectively. These results, shown in **Figure 4** (marked with solid red squares), are consistent with experiments.

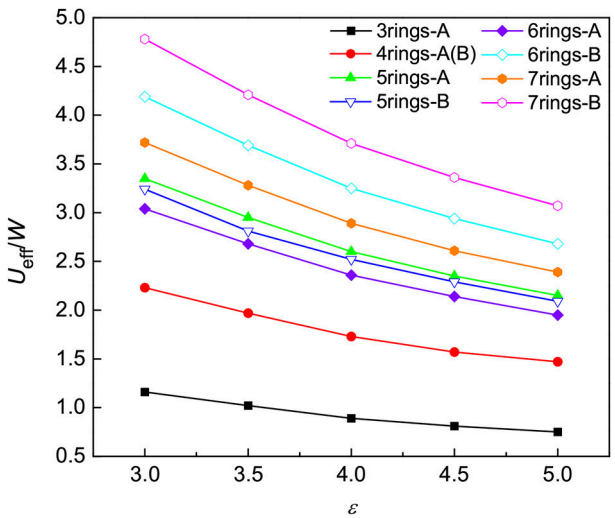

FIGURE 7 | The electron-electron correlations of aromatic hydrocarbons. The effective electronic correlation parameter U_{eff}/W of two kinds of optimized structures is plotted as a function of the dielectric constant ε. The configuration with the zigzag arrangement of benzene rings is classified as A, such as phenanthrene and picene, while B denotes the configuration with the arrangement of benzene rings such as 1,2:8,9-dibenzpentacene and 1,2:5,6-dibenzanthracene.

3.3. Electronic Correlations

In this section we address mechanism for high-T_c phases. Although electron-phonon interaction is still possible to account for higher transition temperatures with certain crystal structure, other possibilities exist. Like other superconductors such as cuprates, further investigations indicate that the electron-electron correlations seem to play an important role on

superconductivity in these systems. In fact, this was similar to charge-transfer organic superconductors [32–37] and fullerides [3, 38], where the importance of electron correlations on superconductivity was emphasized. Magnetic measurements [8] on phenanthrene suggest the existence of local spin moments and indicate similar interplay between magnetism and superconductivity observed in fullerides [3].

To gain some insights on the exchange-correlation effects of electron-electron (e-e), we have carried out the series of calculations using the hybrid functionals method (HSE) [39, 40]. The exchange-correlation energy E_{xc}^{HSE} was written as

$$E_{xc}^{HSE} = \nu E_x^{HF,SR}(\mu) + (1-\nu) E_x^{PBE,SR}(\mu) + E_x^{PBE,LR}(\mu) + E_c^{PBE}, \quad (1)$$

where μ is a screened Coulomb potential which splits the electron-electron exchange interaction into short-range (SR) and long-range (LR) components, the mixing coefficient ν represents the amount of exact/DFT exchange, indicating the extent of Fock exchange and reflecting the intensity of electronic correlation. Within the framework of the HSE method, the correlation interaction is still presented by the PBE functional form [41], the exchange interaction is separated into two parts—SR and LR. The LR exchange item is also described by PBE functional form, while the SR exchange item further splits into exact exchange and PBE forms. Both μ and ν are adjustable parameters; in this calculation, we adjusted them to investigate the extension of e-e interactions in PAH compounds.

For PAH crystal, the band gap is one of the electronic properties reflected by the exchange-correlation interactions. Usually, the LDA functional underestimates the value of band gap due to the incompletely counting of exchange-correlation effects. As mentioned above, the HSE functional can correct the exchange-correlation interaction in PAH compounds as possible as well. The parameter ν just describes the magnitude of the exchange-correlation effects by fitting the band gap between theoretical values and experimental ones. **Table 1** lists out the parameters of μ and ν fitting experimental band gaps for the typical systems such as solid phenanthrene (3rings-A), chrysene [4rings-A(B)], picene (5rings-A), 1,2:5,6-dibenzanthracene (5rings-B), [6]phenacene (6rings-A), 1,2:7,8-dibenzanthracene (6rings-B), [7]phenacene (7rings-A), and 1,2:8,9-dibenzopentacene (7rings-B), respectively. Results show that the ratio ν of exact/DFT exchange becomes larger with the increase of the number of rings whether μ is 0.1 or 0.2, indicating the enhancement of electronic exchange-correlation interactions with the increase of the number of benzene rings.

Another quantity to calculate is the effective Coulomb interaction, e.g., the Hubbard U. Combining the estimated Hubbard U with the calculated bandwidth of bands crossing the Fermi level (see the computational details in the **Supplementary Material**), we indeed found that the electron-electron correlation becomes important as the number of benzene rings increases, as shown in **Figure 7**. Multi-ring hydrocarbons are in favor of strong correlations and thus tend to have higher T_cs. It is therefore believed that both the electron-phonon interaction and electron-electron correlations work together to enhance T_c of the PAHs with increasing the number of benzene rings.

4. CONCLUSIONS

In summary, carrying out first-principles calculations, we have investigated the crystal structures and possible superconductivity in potassium-doped solid benzene and naphthalene. Furthermore, we have analyzed the stability from formation energy, electronic structures near the Fermi level, and electronic correlations of K-doped PAHs. It was found that: (1) Solid benzene can be superconducting when doping with two K atoms; (2) the low T_c phase of $5-7$ K is a common feature in all aromatic hydrocarbon superconductors—for this unique superconducting phase, the doping level is around two electrons in both short-benzene-ring and long-benzene-ring systems, and the electron-phonon interaction is enough to account; and (3) for higher T_c phases in long-benzene-ring systems, the doping level tends toward three electrons. Both the electron-phonon interaction and electron-electron correlations work together to enhance the T_c in long-benzene-ring systems.

AUTHOR CONTRIBUTIONS

X-JC and H-QL designed research. G-HZ performed calculations. G-HZ, X-JC, and H-QL analyzed the results. G-HZ, X-JC, and H-QL wrote the first draft of the paper and all authors contributed to revisions. All authors reviewed the manuscript.

FUNDING

H-QL acknowledges financial support from NSAF U1530401 and computational resources from the Beijing Computational Science Research Center. The work was also supported by the Basic Research Program of Shenzhen under grant Nos. JCYJ20170818153404696 and JCYJ20180507182445460. Partial calculation was supported by the Special Program for Applied Research on Super Computation of the NSFC-Guangdong Joint Fund (the second phase) under Grant No. U1501501.

ACKNOWLEDGMENTS

The authors thank Z. B. Huang, C. Zhang, X. W. Yan, and C. L. Yang for valuable discussions.

SUPPLEMENTARY MATERIAL

The Supplementary Material for this article can be found online at: https://www.frontiersin.org/articles/10.3389/fphy.2019.00052/full#supplementary-material

REFERENCES

1. Ginzburg V. High-temperature superconductivity-dream or reality? *Sov Phys Usp.* (1976) **19**:174–9. doi: 10.1070/PU1976v019n02ABEH005136
2. Hebard A, Rosseinsky M, Haddon R, Murphy D, Glarum S, Palstra T, et al. Superconductivity at 18 K in potassium-doped C_{60}. *Nature.* (1991) **350**:600–1. doi: 10.1038/350600a0
3. Ganin A, Takabayashi Y, Khimyak Y, Margadonna S, Tamai A, Rosseinsky M, et al. Bulk superconductivity at 38 K in a molecular system. *Nat Mater.* (2008) **7**:367–71. doi: 10.1038/nmat2179
4. Jerome D, Mazaud A, Ribault M, Bechgarrd K. Superconductivity in a synthetic organic conductor $(TMTSF)_2PF_6$. *J Phys.* (1980) **41**:L95–8.
5. Taniguchi H, Miyashita M, Uchiyama K, Satoh K, Mori N, Okamoto H, et al. Superconductivity at 14.2 K in layered organics under extreme pressure. *J Phys Soc Jpn.* (2003) **72**:468–71. doi: 10.1143/JPSJ.72.468
6. Mitsuhashi R, Suzuki Y, Yamanari Y, Mitamura H, Kambe T, Ikeda N, et al. Superconductivity in alkali-metal-doped picene. *Nature.* (2010) **464**:76–9. doi: 10.1038/nature08859
7. Kubozono Y, Mitamura M, Lee X, He X, Yamanari Y, Takahashi Y, et al. Metal-intercalated aromatic hydrocarbons: a new class of carbon-based superconductors. *Phys Chem Chem Phys*. (2011) **13**:16476–93. doi: 10.1039/c1cp20961b
8. Wang X, Liu R, Gui Z, Xie Y, Yan Y, Ying J, et al. Superconductivity at 5 K in alkali-metal-doped phenanthrene. *Nat Commun.* (2011) **2**:507–13. doi: 10.1038/ncomms1513
9. Xue M, Cao T, Wang D, Wu Y, Yang H, Dong X, et al. Superconductivity above 30 K in alkali-metal doped hydrocarbon. *Sci Rep.* (2012) **2**:389. doi: 10.1038/srep00389
10. Takabayashi Y, Menelaou M, Tamura H, Takemori N, Koretsune T, Štefančič A, et al. π-electron S=1/2 quantum spin-liquid state in an ionic polyaromatic hydrocarbon. *Nat Chem.* (2017) **9**:635–43. doi: 10.1038/nchem.2764
11. Romero F, Pitcher M, Hiley C, Whitehead G, Kar S, Ganin A, et al. Redox-controlled potassium intercalation into two polyaromatic hydrocarbon solids. *Nat Chem.* (2017) **9**:644–52. doi: 10.1038/nchem.2765
12. Kozhin V, Kitaigorodskii A. Nizkotemperaturnye issledovaniya struktury aromaticheskikh soedinenii. 4. anizotropiya teplovogo rasshireniya v benzole. *Zh Fiz Khim*. (1955) **29**:2074–5.
13. Thiéry M, Léger J. High-pressure solid-phases of benzene. 1. Raman and x-ray studies of C_6H_6 at 294 K up to 25 GPa. *J Chem Phys.* (1988) **89**:4255–71. doi: 10.1063/1.454809
14. Ciabini L, Santoro M, Gorelli F, Bini R, Schettino V, Raugei S. Triggering dynamics of the high-pressure benzene amorphization. *Nat Mater.* (2007) **6**:39–43. doi: 10.1038/nmat1803
15. Wen X, Hoffmann R, Ashcroft N. Benzene under high pressure: a story of molecular crystals transforming to saturated networks, with a possible intermediate metallic phase. *J Am Chem Soc*. (2011) **13**:9023–35. doi: 10.1021/ja201786y
16. López E, Lucas J, de Andrés J, Albertí M, Bofill J, Bassi D, et al. Cross-section energy dependence of the $[C_6H_6M]^+$ adduct formation between benzene molecules and alkali ions (M = Li, Na, K). *Phys Chem Chem Phys*. (2011) **13**:15977–84. doi: 10.1039/c1cp21889a
17. Kresse G, Furthmuller J. Efficiency of ab-initio total energy calculations for metals and semiconductors using a plane-wave basis set. *Comput Mater Sci*. (1996) **6**:15–50. doi: 10.1016/0927-0256(96)00008-0
18. Kresse G, Furthmuller J. Efficient iterative schemes for ab Initio total-energy calculations using a plane-wave basis set. *Phys Rev B*. (1996) **54**:11169–86. doi: 10.1103/PhysRevB.54.11169
19. Kresse G, Joubert D. From ultrasoft pseudopotentials to the projector augmented-wave method. *Phys Rev B*. (1999) **59**:1758–75. doi: 10.1103/PhysRevB.59.1758
20. Ceperley D, Alder B. Ground state of the electron gas by a stochastic method. *Phys Rev Lett*. (1980) **45**:566–9. doi: 10.1103/PhysRevLett.45.566
21. Perdew J, Zunger A. Self-interaction correction to density-functional approximations for many-electron systems. *Phys Rev B*. (1981) **23**:5048–79. doi: 10.1103/PhysRevB.23.5048
22. Casula M, Calandra M, Profeta G, Mauri F. Intercalant and intermolecular phonon assisted superconductivity in K-doped picene. *Phys Rev Lett*. (2011) **107**:137006. doi: 10.1103/PhysRevLett.107.137006
23. Giannozzi P, Baroni S, Bonini N, Calandra M, Car R, Cavazzoni C, et al. QUANTUM ESPRESSO: a modular and open-source software project for quantum simulations of materials. *J Phys Condens Matter*. (2009) **21**:395502. doi: 10.1088/0953-8984/21/39/395502
24. Troullier N, Martins J. Efficient pseudopotentials for plane-wave calculations. *Phys Rev B*. (1991) **43**:1993–2006. doi: 10.1103/PhysRevB.43.1993
25. Weller T, Ellerby M, Saxena S, Smith P, Skipper N. Superconductivity in the intercalated graphite compounds C_6Yb and C_6Ca. *Nat Phys*. (2005) **1**:39–41.
26. Emery N, Hérold C, d'Astuto M, Garcia V, Bellin C, Marêché J, et al. Superconductivity of bulk CaC_6. *Phys Rev Lett*. (2005) **95**:087003. doi: 10.1103/PhysRevLett.95.087003
27. Kato T, Kambe T, Kubozono Y. Strong intramolecular electron-phonon coupling in the negatively charged aromatic superconductor picene. *Phys Rev Lett*. (2011) **107**:077001. doi: 10.1103/PhysRevLett.107.077001
28. Allen P, Dynes R. Transition temperature of strong-coupled superconductors reanalyzed. *Phys Rev B*. (1975) **12**:905–22. doi: 10.1103/PhysRevB.12.905
29. Hannay N, Geballe T, Matthias B, Andres K, Schmidt P, MacNair D. Superconductivity in graphitic compounds. *Phys Rev Lett*. (1965) **14**:225–6. doi: 10.1103/PhysRevLett.14.225
30. Wang X, Zhong G, Yan X, Chen X, Lin H. First-principles prediction on geometrical and electronic properties of K-doped chrysene. *J Phys Chem Solids*. (2017) **104**:56–61. doi: 10.1016/j.jpcs.2017.01.004
31. Artioli G, Hammerath F, Mozzati M, Carretta P, Corana F, Mannucci B, et al. Superconductivity in Sm-doped [n]phenacenes (n = 3, 4, 5). *Chem Commun*. (2015) **51**:1092–5. doi: 10.1039/C4CC07879A
32. Kivelson S, Chapman O. Polyacene and a new class of quasi-one-dimensional conductors. *Phys Rev B*. (1983) **28**:7236–43. doi: 10.1103/PhysRevB.28.7236
33. Karakonstatakis G, Berg E, White S, Kivelson S. Enhanced pairing in the checkerboard Hubbard ladder. *Phys Rev B*. (2011) **83**:054508. doi: 10.1103/PhysRevB.83.054508
34. Giovannetti G, Capone M. Electronic correlation effects in superconducting picene from *ab* initio calculations. *Phys Rev B*. (2011) **83**:134508. doi: 10.1103/PhysRevB.83.134508
35. Huang Z, Zhang C, Lin H. Magnetic instability and pair binding in aromatic hydrocarbon superconductors. *Sci Rep*. (2012) **2**:922. doi: 10.1038/srep00922
36. Kim M, Min B, Lee G, Kwon H, Rhee Y, Shim J. Density functional calculations of electronic structure and magnetic properties of the hydrocarbon K_3picene superconductor near the metal-insulator transition. *Phys Rev B*. (2011) **83**:214510. doi: 10.1103/PhysRevB.83.214510
37. Ruff A, Sing M, Claessen R, Lee H, Tomic M, Jeschke H, et al. Absence of metallicity in K-doped picene: importance of electronic correlations. *Phys Rev Lett*. (2013) **110**:216403. doi: 10.1103/PhysRevLett.110.216403
38. Duband P, Darling G, Dubitsky Y, Zaopo A, Rosseinsky M. The Mott-Hubbard insulating state and orbital degeneracy in the superconducting C_{60}^{3-} fulleride family. *Nat Mater*. (2003) **2**:605–10. doi: 10.1038/nmat953
39. Heyd J, Scuseria G, Ernzerhof M. Hybrid functionals based on a screened Coulomb potential. *J Chem Phys*. (2003) **118**:8207–15. doi: 10.1063/1.1564060
40. Heyd J, Scuseria G. Efficient hybrid density functional calculations in solids: assessment of the Heyd-Scuseria-Ernzerhof screened Coulomb hybrid functional. *J Chem Phys*. (2004) **121**:1187. doi: 10.1063/1.1760074
41. Perdew J, Burke K, Ernzerhof M. Generalized gradient approximation made simple. *Phys Rev Lett*. (1996) **77**:3865. doi: 10.1103/PhysRevLett.77.3865
42. Bhatti M, Ali M, Shahid G, Saleh M. Characterization of phenanthrene single crystals. *Turk J Phy*. (2000) **24**:673–9.
43. Roth F, Mahns B, Schofelder R, Hampel S, Nohr M, Buchner B, et al. Comprehensive studies of the electronic structure of pristine and potassium doped chrysene investigated by electron energy-loss spectroscopy. *J Chem Phys*. (2012) **137**:114508. doi: 10.1063/1.4753999
44. Okamoto H, Kawasaki N, Kaji Y, Kubozono Y, Fujiwara A, Yamaji M. Air-assisted high-performance field-effect transistor with thin films of picene. *J Am Chem Soc*. (2008) **130**:10470–1. doi: 10.1021/ja803291a

45. Chang N, Mori H, Chen X, Okuda Y, Okamoto T, Nishihara Y. Synthesis of substituted [6]Phenacenes through suzuki-miyaura coupling of polyhalobenzene with alkenylboronates and sequential intramolecular cyclization via C-H bond activation. *Chem Lett*. (2013) **42**:1257–9. doi: 10.1246/cl.130584
46. Roth F, Konig A, Mahns B, Buchner B, Knupfer M. Evidence for phase formation in potassium intercalated 1,2;8,9-dibenzopentacene. *Eur Phys J B*. (2012) **85**:242. doi: 10.1140/epjb/e2012-30247-3

Conflict of Interest Statement: The authors declare that the research was conducted in the absence of any commercial or financial relationships that could be construed as a potential conflict of interest.